Simplified modeling strategies for soil-structure interaction problems: The multifiber beam concept

Panagiotis Kotronis

Simplified modeling strategies for soil-structure interaction problems: The multifiber beam concept

Panagiotis Kotronis

LUNAM Université, Ecole Centrale de Nantes, Université de Nantes, CNRS UMR 6183, GeM (Institut de Recherche en Génie Civil et Mécanique), 1 rue de la Noë, BP 92101, 44321, Nantes, cedex 3, France

---

Starting with the study of different Euler Bernoulli and Timoshenko beam finite element formulations, a displacement based multifiber Timoshenko beam is presented. The element is free of shear locking problems and it is able to reproduce the non linear behaviour of composite structures. It is validated using the experimental results of a reinforced concrete viaduct subjected to earthquake loadings. Despite the small number of degrees of freedom of the finite element model, the non linear behaviour of the viaduct is predicted satisfactorily. Not only the peaks in both directions are well reproduced but the frequency content of the response is correctly matched. Multifiber beams combined with macro-elements [Gra13] can take into account in a efficient, fast and robust way soil-structure interaction phenomena. This is shown in the last section of the article where the influence of the soil-structure interaction on the behaviour of the reinforced viaduct is highlighted.

1 Introduction

The objective of this course is to introduce the differences between the Euler Bernoulli and Timoshenko theories, to present various finite element beam formulations and to show the equations of displacement based Timoshenko multifiber beam elements. The paper follows mainly the work and ideas exposed in [Peg94], [GPP94], [KM05], [MKRC06], [Bit13], [CKCed]. The important subject of force based beam finite elements is not discussed hereafter. The reader can find information on this subject in the following references [SFT96a], [SFT96b].

2 Classical beam theories

2.1 Kinematics

We consider hereafter a beam of length L and section $S(x)$ (figure 1). $G(x, y, z)$ is the center of gravity of the section $S(x)$ and $P(x, y, z)$ a point in the section. We define as neutral axis the line that links the center of gravities of all the sections. We also suppose that G_x, G_y, G_z are principal axes. For the 2D case studied hereafter (loadings are in the $x - y$ plane), the displacements $\underline{\mathbf{u}}^T = \{u_x, u_y\}$ of the point $P(x, y, z)$ can be expressed as a function of the displacements $U_x(x), U_y(x)$ and the rotation $\Theta_z(x)$ of the section $S(x)$ (often defined in the literature as *generalised* displacements, see also equations (8) and (16)) considering the following two kinematic hypotheses:

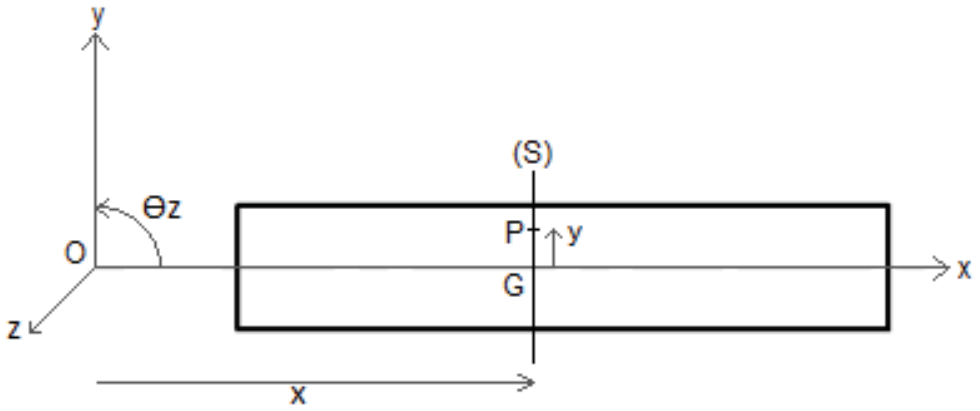

Figure 1: Beam [Bit13]

- Euler Bernoulli theory: In this theory, the section remains plane and perpendicular to the neutral axis (figure 2).

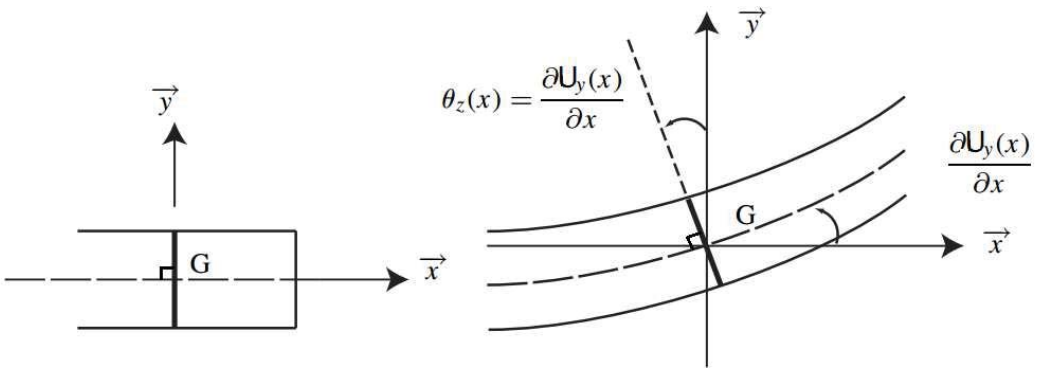

Figure 2: Euler Bernoulli theory [Bit13]

A consequence of the previous kinematic assumption is that the rotation of the section $\Theta_z(x)$ equals $U'_y(x)$ (the symbol $'$ defines hereafter the first derivative with respect to x and the symbol $''$ the second derivative with respect to x)

(figure 2). The displacements of the point $P(x, y, z)$ take thus the following form [GPP94]:

$$\begin{aligned} u_x(x, y) &= U_x(x) - y\Theta_z(x) = U_x(x) - yU'_y(x) \\ u_y(x, y) &= U_y(x) \end{aligned} \tag{1}$$

and the strains are calculated as (infinitesimal strain theory assumption):

$$\begin{aligned} \varepsilon_x &= \frac{\partial u_x}{\partial x} = U'_x(x) - y\Theta'_z(x) = U'_x(x) - yU''_y(x) \\ \gamma_{xy} &= \frac{\partial u_x}{\partial y} + \frac{\partial u_y}{\partial x} = U'_y(x) - \Theta_z(x) = 0 \end{aligned} \tag{2}$$

One can notice that due to the adopted kinematic hypothesis shear strains are found equal to zero.

- Timoshenko theory: In this theory, the kinematic assumption is that the section remains plane but not necessarily perpendicular to the neutral axis. In other words, $\Theta_z \neq U'_y(x)$, see figure 3. Displacements and strains (infinitesimal strain theory assumption) are now calculated as [GPP94]:

$$\begin{aligned} u_x(x, y) &= U_x(x) - y\Theta_z(x) \\ u_y(x, y) &= U_y(x) \end{aligned} \tag{3}$$

$$\begin{aligned} \varepsilon_x &= \frac{\partial u_x}{\partial x} = U'_x(x) - y\Theta'_z(x) \\ \gamma_{xy} &= \frac{\partial u_x}{\partial y} + \frac{\partial u_y}{\partial x} = U'_y(x) - \Theta_z(x) \end{aligned} \tag{4}$$

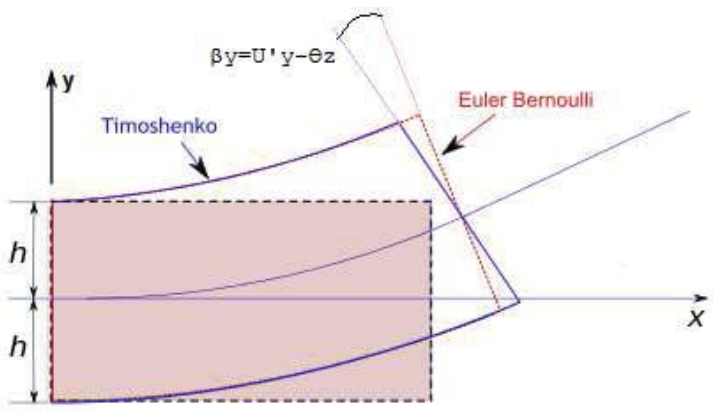

Figure 3: Timoshenko theory (Wikipedia)

We define hereafter

$$\beta_y = U'_y(x) - \Theta_z(x) \tag{5}$$

The variable β_y represents the rotation of the section due to shear. From equation (4) one can notice that shear strains are now constant in the section (and not as in the Euler Bernoulli theory necessarily equal to zero).

2.2 Euler Bernoulli theory: Principal work principle and generalised forces

The virtual work principle is written as (body forces and inertial forces are hereafter neglected. The symbol σ defines stresses):

$$\int_0^L \int_S \delta\varepsilon_x \sigma_x dS dx - w_{exter} = 0 \tag{6}$$

with w_{exter} the work of the external forces.

Replacing (2) in (6) we get:

$$\int_0^L \int_S \delta(U'_x(x) - y\Theta'_z(x))\sigma_x dS dx - w_{exter} = 0 \tag{7}$$

We define hereafter the *generalised* forces in the section as:

$$\begin{aligned} &\text{Normal force: } F_x = \int_S \sigma_x dS \\ &\text{Bending moment : } M_z = -\int_S y\sigma_x dS \end{aligned} \tag{8}$$

and equation (7) becomes:

$$\int_0^L (F_x \delta U'_x + M_z \delta\Theta'_z) dx - w_{exter} = 0 \tag{9}$$

Within a beam theory $\sigma_y = \sigma_z = \sigma_{yz} = 0$. Furthermore and because of equation (2) $\sigma_{xz} = \sigma_{xy} = 0$. Hooke's law thus becomes (with E the Young's modulus and ν the Poisson's coefficient):

$$\begin{aligned} \sigma_x &= E\varepsilon_x \\ \varepsilon_y &= \varepsilon_z = -\nu\varepsilon_x \end{aligned} \tag{10}$$

Finally, using equations (2), (8) and (10) the generalised forces become:

$$F_x = \int_S E\varepsilon_x dS = \int_S E(U'_x(x) - y\Theta'_z(x))dS = \int_S EU'_x(x)dS = ESU'_x(x)$$
$$M_z = -\int_S yE\varepsilon_x dS = -\int_S yE(U'_x(x) - y\Theta'_z(x))dS = \int_S y^2 E\Theta'_z(x)dS = EI_z\Theta'_z(x) \tag{11}$$

Remarks:

- The axis z is a principal axis and therefore $\int_S ydS = 0$.
- An homogeneous section is considered.

Introducing equation (11) in the virtual work principle (9) we have:

$$\int_0^L (\delta U'_x(x)ESU'_x(x) + \delta\Theta'_z(x)EI\Theta'_z(x))dx - w_{exter} = 0 \tag{12}$$

If $\underline{\mathbf{F_s}}^T = \{F_x, M_z\}$ the generalised force vector and $\underline{\mathbf{D_s}}^T = \{U'_x, \Theta'_z\}$ the generalised displacement vector we define the stiffness matrix of the section $\underline{\underline{\mathbf{K_s}}}$ as:

$$\underline{\mathbf{F_s}} = \underline{\underline{\mathbf{K_s}}}\,\underline{\mathbf{D_s}} = \begin{Bmatrix} F_x \\ M_z \end{Bmatrix} = \begin{bmatrix} ES & 0 \\ 0 & EI_z \end{bmatrix} \begin{Bmatrix} U'_x \\ \Theta'_z \end{Bmatrix} = \begin{bmatrix} ES & 0 \\ 0 & EI_z \end{bmatrix} \begin{Bmatrix} U'_x \\ U''_y \end{Bmatrix} \tag{13}$$

2.3 Timoshenko theory: Principal work principle and generalised forces

The principle work principle now becomes:

$$\int_0^L \int_S (\delta\varepsilon_x\sigma_x + 2\delta\varepsilon_{xy}\sigma_{xy})dSdx - w_{exter} = 0 \tag{14}$$

Using equation (4) we get:

$$\int_0^L \int_S (\delta(U'_x(x) - y\Theta'_z(x))\sigma_x + (\delta U'_y(x) - \delta\Theta_z(x))\sigma_{xy}dSdx - w_{exter} = 0 \tag{15}$$

where the generalised forces are:

$$\begin{aligned} &\text{Normal force: } F_x = \int_S \sigma_x dS \\ &\text{Shear force: } F_y = \int_S \sigma_{xy} dS \\ &\text{Bending moment : } M_z = -\int_S y\sigma_x dS \end{aligned} \tag{16}$$

Equation (15) becomes:

$$\int_0^L (F_x \frac{d}{dx}\delta U_x + F_y \frac{d}{dx}\delta\beta_y + M_z \frac{d}{dx}\delta\Theta_z)dx - w_{exter} = 0 \tag{17}$$

Using Hooke's law ($\sigma_x = E\varepsilon_x, \sigma_{xy} = G\gamma_{xy}$, with G the shear coefficient) we obtain:

$$F_x = \int_S \sigma_x dS = \int_S E\varepsilon_x dS = \int_S E(\frac{dU_x}{dx} - y\frac{d\Theta_z}{dx})dS = \int_S EU'_x ds = ESU'_x \tag{18}$$

In a similar way we have:

$$\begin{aligned} F_y &= GS\beta_y \\ M_z &= EI_z\Theta'_z \end{aligned} \tag{19}$$

If $\underline{\mathbf{F_s}}^T = \{F_x, F_y, M_z\}$ the generalised force vector and $\underline{\mathbf{D_s}}^T = \{U'_x, \beta_y, \Theta'_z\}$ the generalised strain vector we define the stiffness matrix of the section $\underline{\underline{\mathbf{K_s}}}$ as:

$$\underline{\mathbf{F_s}} = \underline{\underline{\mathbf{K_s}}}\,\underline{\mathbf{D_s}} = \begin{Bmatrix} F_x \\ F_y \\ M_z \end{Bmatrix} = \begin{bmatrix} ES & 0 & 0 \\ 0 & GS & 0 \\ 0 & 0 & EI_z \end{bmatrix} \begin{Bmatrix} U'_x \\ \beta_y \\ \Theta'_z \end{Bmatrix} \tag{20}$$

Remark: The Timoshenko beam theory provides constant shear strains and stresses in the section (see equation (4) and Hooke's law). This result violates the boundary conditions of the beam theory ($\sigma_y = \sigma_z = 0$) and does not agree with the theoretical distribution of stresses which is parabolic for a rectangular cross section. A simplified way to deal with this inconsistency is to change the definition of the shear force by adding a shear corrector factor (or Reissner corrector factor) k that depends on the cross section geometry and the material characteristics [Cow66]. The modified expressions take thus the following form:

$$\text{Shear force: } F_y = \int_S k\sigma_{xy} dS \tag{21}$$

$$\underline{\mathbf{F_s}} = \underline{\underline{\mathbf{K_s}}}\,\underline{\mathbf{D_s}} = \begin{Bmatrix} F_x \\ F_y \\ M_z \end{Bmatrix} = \begin{bmatrix} ES & 0 & 0 \\ 0 & kGS & 0 \\ 0 & 0 & EI_z \end{bmatrix} \begin{Bmatrix} U'_x \\ \beta_y \\ \Theta'_z \end{Bmatrix} \tag{22}$$

2.4 A 2 node beam finite element formulation

Consider a 2D beam finite element with two nodes and three degrees of freedom per node (figure 4).

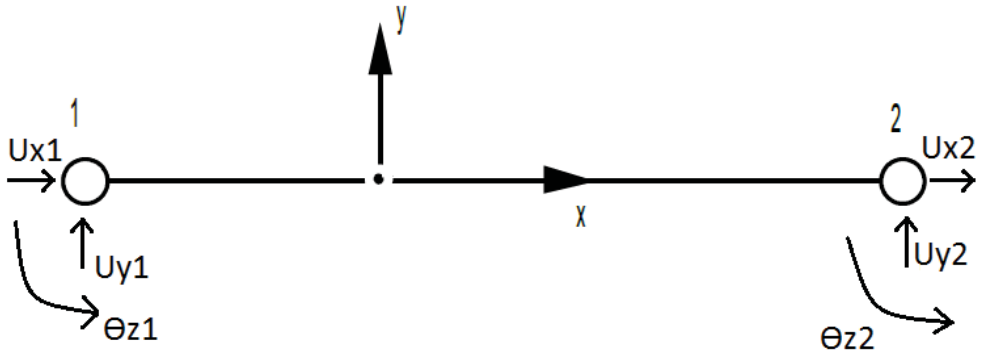

Figure 4: A 2 node finite element beam [Bit13]

Displacements $U_x(x), U_y(x)$ and rotations $\Theta_z(x)$ along the beam are discretized using the nodal displacements as follows:

$$\underline{\mathbf{U}} = \underline{\underline{\mathbf{N}}}\,\underline{\mathbf{\Phi}} \tag{23}$$

or

$$\begin{Bmatrix} U_x \\ U_y \\ \Theta_z \end{Bmatrix} = \begin{bmatrix} N1 & N2 & N3 & N4 & N5 & N6 \\ N7 & N8 & N9 & N10 & N11 & N12 \\ N13 & N14 & N15 & N16 & N17 & N18 \end{bmatrix} \begin{Bmatrix} U_{x1} \\ U_{y1} \\ \Theta_{z1} \\ U_{x2} \\ U_{y2} \\ \Theta_{z2} \end{Bmatrix} \tag{24}$$

where $N_i(x), i = 1, 18$ the shape functions and $\underline{\mathbf{\Phi}}$ the nodal displacements. The equation providing the generalised strain vector $\underline{\mathbf{D_s}}$ becomes (a for axial, s for shear and b for bending):

$$\begin{aligned} \underline{\mathbf{D_s}} = \begin{Bmatrix} U_x' \\ \beta_y \\ \Theta_z' \end{Bmatrix} &= \begin{bmatrix} B1 & B2 & B3 & B4 & B5 & B6 \\ B7 & B8 & B9 & B10 & B11 & B12 \\ B13 & B14 & B15 & B16 & B17 & B18 \end{bmatrix} \begin{Bmatrix} U_{x1} \\ U_{y1} \\ \Theta_{z1} \\ U_{x2} \\ U_{y2} \\ \Theta_{z2} \end{Bmatrix} \\ &= \begin{bmatrix} B_a \\ B_s \\ B_b \end{bmatrix} \begin{Bmatrix} U_{x1} \\ U_{y1} \\ \Theta_{z1} \\ U_{x2} \\ U_{y2} \\ \Theta_{z2} \end{Bmatrix} \end{aligned} \tag{25}$$

Using the previous equation in the virtual work principle we get a system of linear equations that take the following form (with $\underline{\mathbf{F}}$ the vector of nodal forces at the element level and $\underline{\underline{\mathbf{K_e}}}$ the element stiffness matrix):

$$\underline{\mathbf{F}} = \underline{\underline{\mathbf{K_e}}}\ \underline{\mathbf{\Phi}} \tag{26}$$

The element stiffness matrix $\underline{\underline{\mathbf{K_e}}}$ is given by (where the symbol $+$ means matrix assembly, adding in an adequate way the different degrees of freedom) :

$$\underline{\underline{\mathbf{K_e}}} = \underline{\underline{\mathbf{K_a}}} + \underline{\underline{\mathbf{K_s}}} + \underline{\underline{\mathbf{K_b}}} \tag{27}$$

$$\begin{aligned} \underline{\underline{\mathbf{K_a}}} &= \int_0^L B_a^T E S B_a dx \\ \underline{\underline{\mathbf{K_s}}} &= \int_0^L B_s^T k G S B_s dx \\ \underline{\underline{\mathbf{K_b}}} &= \int_0^L B_b^T E I B_b dx \end{aligned} \tag{28}$$

2.4.1 An Euler Bernoulli 2 node finite element beam

Consider for example the following classical shape functions for the horizontal, vertical and rotational degrees of freedom [Fre00]:

$$\begin{gathered} N_1 = 1 - \frac{x}{l} \ \ and \ \ N_4 = \frac{x}{l} \\ N_8 = 1 - 3(\frac{x}{l})^2 + 2(\frac{x}{l})^3 \ \ and \ \ N_9 = x - 2\frac{x^2}{l} + \frac{x^3}{l^2} \\ N_{11} = 3(\frac{x}{l})^2 - 2(\frac{x}{l})^3 \ \ and \ \ N_{12} = -\frac{x^2}{l} + \frac{x^3}{l^2} \\ N_{14} = N_8' \ \ and \ \ N_{15} = N_9' \\ N_{17} = N_{11}' \ \ and \ \ N_{18} = N_{12}' \end{gathered} \tag{29}$$

In this formulation the rotational and vertical displacements are made interdependent. The other shape functions are considered equal to zero and so equation (24) becomes:

$$\begin{Bmatrix} U_x \\ U_y \\ \theta_z \end{Bmatrix} = \begin{bmatrix} N_1 & 0 & 0 & N_4 & 0 & 0 \\ 0 & N_8 & N_9 & 0 & N_{11} & N_{12} \\ 0 & N_8' & N_9' & 0 & N_{11}' & N_{12}' \end{bmatrix} \begin{Bmatrix} U_{x_1} \\ U_{y_1} \\ \Theta_{z_1} \\ U_{x_2} \\ U_{y_2} \\ \Theta_{z_2} \end{Bmatrix} \tag{30}$$

The different stiffness matrices, for a constant homogeneous section S, take the following form (the matrix due to shear is equal to the zero matrix):

$$\begin{aligned}\underline{\underline{\mathbf{K_a}}} &= \frac{ES}{l}\begin{bmatrix}1 & -1\\ -1 & 1\end{bmatrix}\\ \underline{\underline{\mathbf{K_b}}} &= \frac{EI}{l^3}\begin{bmatrix}12 & 6l & -12 & 6l\\ 6l & 4l^2 & -6l & 2l^2\\ -12 & -6l & 12 & -6l\\ 6l & 2l^2 & -6l & 4l^2\end{bmatrix}\end{aligned} \tag{31}$$

$$\underline{\underline{\mathbf{K_e}}} = \begin{bmatrix} ES/l & 0 & 0 & -ES/l & 0 & 0\\ 0 & 12EI/l^3 & 6EI/l^2 & 0 & -12EI/l^3 & 6EI/l^2\\ 0 & 6EI/l^2 & 4EI/l & 0 & -6EI/l^2 & 2EI/l\\ -ES/l & 0 & 0 & ES/l & 0 & 0\\ 0 & -12EI/l^3 & -6EI/l^2 & 0 & 12EI/l^3 & -6EI/l^2\\ 0 & 6EI/l^2 & 2EI/l & 0 & -6EI/l^2 & 4EI/l \end{bmatrix} \tag{32}$$

2.4.2 A Timoshenko 2 node finite element beam (1st formulation)

For the case of a Timoshenko beam finite element, the choice of the shape functions is crucial because of the possible shear locking numerical problem [HTK77], [DL87], [ZT05]. If these functions are not appropriately chosen, the finite element beam presents a spurious stiffness for the case of elongated beams. A simple adequate set of shape functions is presented hereafter [Peg94], [GPP94]:

$$\begin{aligned} N_1 = N_8 = N_{15} &= \frac{x_2 - x}{L}\\ N_4 = N_{11} = N_{18} &= \frac{x - x_1}{L}\end{aligned} \tag{33}$$

$$\begin{Bmatrix} U_x\\ U_y\\ \theta_z \end{Bmatrix} = \begin{bmatrix} N_1 & 0 & 0 & N_4 & 0 & 0\\ 0 & N_8 & 0 & 0 & N_{11} & 0\\ 0 & 0 & N_{15} & 0 & 0 & N_{18}\end{bmatrix} \begin{Bmatrix} U_{x_1}\\ U_{y_1}\\ \Theta_{z_1}\\ U_{x_2}\\ U_{y_2}\\ \Theta_{z_2}\end{Bmatrix} \tag{34}$$

The generalised strains become:

$$\underline{\mathbf{D_s}} = \begin{bmatrix} B_a\\ B_s\\ B_b\end{bmatrix} \underline{\mathbf{\Phi}} = \begin{bmatrix} -\frac{1}{l} & 0 & 0 & \frac{1}{l} & 0 & 0\\ 0 & -\frac{1}{l} & -\frac{x_2-x}{l} & 0 & \frac{1}{l} & -\frac{x-x_1}{l}\\ 0 & 0 & -\frac{1}{l} & 0 & 0 & \frac{1}{l}\end{bmatrix} \begin{Bmatrix} U_{x_1}\\ U_{y_1}\\ \Theta_{z_1}\\ U_{x_2}\\ U_{y_2}\\ \Theta_{z_2}\end{Bmatrix} \tag{35}$$

In order to avoid shear locking problems, [DL87] propose to eliminate the linear term in B_s or [HTK77] to sub-integrate the $\underline{\underline{\mathbf{K_s}}}$ using only 1 Gauss integration point. According to the solution proposed by [DL87], [GPP94], β_y is now corrected as:

$$\overline{\beta}_y = -\frac{1}{l}U_{y_1} - \frac{1}{2}\Theta_{z_1} + \frac{1}{l}U_{y_2} - \frac{1}{2}\Theta_{z_2} = \overline{B}_s\underline{\mathbf{\Phi}} \tag{36}$$

Finally, the element stiffness matrix, for a constant homogeneous section, takes the following form:

$$\underline{\underline{\mathbf{K_e}}} = \begin{bmatrix} \frac{ES}{L} & 0 & 0 & -\frac{ES}{L} & 0 & 0 \\ 0 & \frac{kSG}{L} & \frac{kSG}{2} & 0 & -\frac{kSG}{L} & \frac{kSG}{2} \\ 0 & \frac{kSG}{2} & \frac{EI}{L} + \frac{kSGL}{4} & 0 & -\frac{kSG}{2} & -\frac{EI}{L} + \frac{kSGL}{4} \\ -\frac{ES}{L} & 0 & 0 & \frac{ES}{L} & 0 & 0 \\ 0 & -\frac{kSG}{L} & -\frac{kSG}{2} & 0 & \frac{kSG}{L} & -\frac{kSG}{2} \\ 0 & \frac{kSG}{2} & -\frac{EI}{L} + \frac{kSGL}{4} & 0 & -\frac{kSG}{2} & \frac{EI}{L} + \frac{kSGL}{4} \end{bmatrix} \tag{37}$$

2.4.3 A Timoshenko 2 node finite element beam (2nd formulation)

Another way to avoid shear locking problems is to use higher order functions and to integrate exactly the stiffness matrix. For a 2 node finite element this leads to shape functions that depend on the material properties [DVdG89], [FK93], [KM05], [MKRC06]. For example, according to [FK93] the shape functions become:

$$\underline{\underline{\mathbf{N}}} = \begin{bmatrix} N_1 & 0 & 0 & N_4 & 0 & 0 \\ 0 & N_8 & N_9 & 0 & N_{11} & N_{12} \\ 0 & N_{14} & N_{15} & 0 & N_{17} & N_{18} \end{bmatrix} \tag{38}$$

with:

$$
\begin{aligned}
N_1 =& 1 - \frac{x}{L} \\
N_4 =& \frac{x}{L} \\
N_8 =& \frac{1}{1+\phi}[2(\frac{x}{L})^3 - 3(\frac{x}{L})^2 - \phi(\frac{x}{L}) + 1 + \phi] \\
N_9 =& \frac{L}{1+\phi}[(\frac{x}{L})^3 - (2+\frac{\phi}{2})(\frac{x}{L})^2 + (1+\frac{\phi}{2})(\frac{x}{L})] \\
N_{11} =& \frac{-1}{1+\phi}[2(\frac{x}{L})^3 - 3(\frac{x}{L})^2 - \phi(\frac{x}{L})] \\
N_{12} =& \frac{L}{1+\phi}[(\frac{x}{L})^3 - (1-\frac{\phi}{2})(\frac{x}{L})^2 - \frac{\phi}{2}(\frac{x}{L})] \\
N_{14} =& \frac{6}{(1+\phi)L}[(\frac{x}{L})^2 - (\frac{x}{L})] \\
N_{15} =& \frac{1}{1+\phi}[3(\frac{x}{L})^2 - (4+\phi)(\frac{x}{L}) + (1+\phi)] \\
N_{17} =& \frac{-6}{(1+\phi)L}[(\frac{x}{L})^2 - (\frac{x}{L})] \\
N_{18} =& \frac{L}{1+\phi}[3(\frac{x}{L})^2 - (2-\phi)(\frac{x}{L})]
\end{aligned}
\tag{39}
$$

ϕ is the ratio between bending and shear stiffnesses. For an homogeneous section we get:

$$
\phi = \frac{12}{L^2}\,\frac{\int_S Ey^2 dS}{\int_S kG dS} = \frac{12}{L^2}\,\frac{EI}{kGS} \tag{40}
$$

The generalised strains now become:

$$
\underline{\mathbf{D_s}} = \begin{bmatrix} N_1' & 0 & 0 & N_4' & 0 & 0 \\ 0 & N_8' - N_{14} & N_9' - N_{15} & 0 & N_{11}' - N_{17} & N_{12}' - N_{18} \\ 0 & N_{14}' & N_{15}' & 0 & N_{17}' & N_{18}' \end{bmatrix} \begin{Bmatrix} U_{x_1} \\ U_{y_1} \\ \Theta_{z_1} \\ U_{x_2} \\ U_{y_2} \\ \Theta_{z_2} \end{Bmatrix} \tag{41}
$$

Finally, the stiffness matrix of the element takes the following form:

$$\underline{\underline{\mathbf{K_e}}} = \begin{bmatrix} \frac{ES}{L} & 0 & 0 & -\frac{ES}{L} & 0 & 0 \\ 0 & \frac{12EI}{(1+\phi)L^3} & \frac{6EI}{(1+\phi)L^2} & 0 & -\frac{12EI}{(1+\phi)L^3} & \frac{6EI}{(1+\phi)L^2} \\ 0 & \frac{6EI}{(1+\phi)L^2} & \frac{(4+\phi)EI}{(1+\phi)L} & 0 & -\frac{6EI}{(1+\phi)L^2} & \frac{(2-\phi)EI}{(1+\phi)L} \\ -\frac{ES}{L} & 0 & 0 & \frac{ES}{L} & 0 & 0 \\ 0 & -\frac{12EI}{(1+\phi)L^3} & -\frac{6EI}{(1+\phi)L^2} & 0 & \frac{12EI}{(1+\phi)L^3} & -\frac{6EI}{(1+\phi)L^2} \\ 0 & \frac{6EI}{(1+\phi)L^2} & \frac{(2-\phi)EI}{(1+\phi)L} & 0 & -\frac{6EI}{(1+\phi)L^2} & \frac{(4+\phi)EI}{(1+\phi)L} \end{bmatrix} \quad (42)$$

For elongated beams, ϕ is almost zero and the matrix reduces to the classical Euler Bernoulli stiffness matrix, see equation (32). The main problem of this finite element formulation is that it is not appropriate for non linear calculations as the shape functions depend on the material properties that evolve with the loading. Nevertheless, some good results where obtained by keeping the initial shape functions (calculated at the first step - elasticity) unchanged, [KM05], [MKRC06].

2.4.4 Timoshenko finite elements with internal degrees of freedom

Another way to avoid shear locking problems is to enrich the displacements field [IW91] and to add internal nodes in the element [IF93], [CKCed]. In that way higher order shape functions are obtained that do not depend on the material properties. The numerical integration is exactly performed and the elements are suitable for non linear calculations.

The finite element presented in [CKCed] (named "FCQ" Timoshenko beam for "Full Cubic Quadratic") has additional internal degrees of freedom, cubic shape functions for the vertical displacements and quadratic for the rotations. The element is free of shear locking and one element is able to predict the exact tip displacements for any complex distributed loadings and any suitable boundary conditions. One element gives the exact solution for the case of bending of a Timoshenko beam free of distributed loadings. It is also proven that the element presented in [FK93] is a particular case of the more general FCQ Timoshenko beam element. For more information the reader is invited to read the relevant reference.

3 Multifiber beam formulation

The section of the finite element beam (Euler Bernoulli or Timoshenko) is divided in different "fibers" [OH80]. In each fiber a constitutive law is introduced (e.g. concrete,

steel...). Depending on the mesh discretization of the section (e.g. with triangular or rectangular finite elements) one or more Gauss points are associated in each fiber, see figure 5.

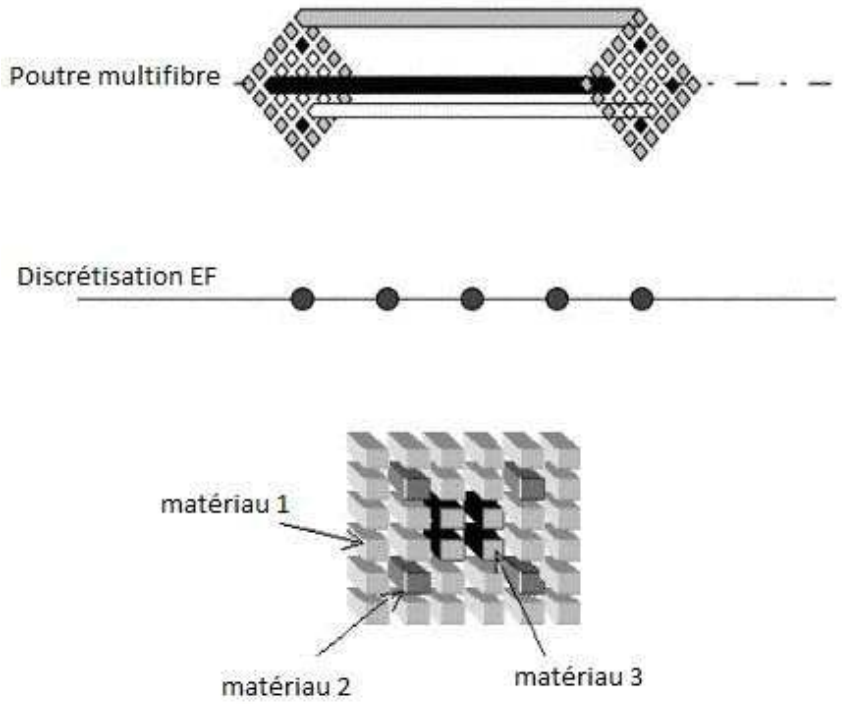

Figure 5: Multifiber beam modelling [GPP94], [MKRC06]

The different formulations of the finite element beams presented in section 2 (expressed now in 3D) can be used for the multifiber element. Consider equations (1) and (3) expressing the kinematic assumptions: the y (and z in 3D) are replaced with y_f (and z_f), the coordinates of the fiber f in the section. The generalised forces take the following forms (where E_f and G_f the Young's and the shear moduli of the fiber respectively):

$$F_x = \int_S E_f \varepsilon_x dS = \int_S E_f (\frac{dU_x}{dx} - y_f \frac{d\Theta_z}{dx}) dS = \int_S E_f dS U'_x - \int_S E_f y_f dS \Theta'_z \tag{43}$$

and in a similar way:

$$\begin{Bmatrix} F_x \\ F_y \\ M_z \end{Bmatrix} = \begin{bmatrix} \int_S E_f dS & 0 & -\int_S E_f y_f dS \\ 0 & \int_S k G_f dS & 0 \\ -\int_S E_f y_f dS & & \int_S E_f y_f^2 dS \end{bmatrix} \begin{Bmatrix} U'_x \\ \beta_y \\ \Theta_z \end{Bmatrix} \tag{44}$$

By introducing the previous equation of the virtual work principle we obtain:

$$\int_0^L \delta \underline{\mathbf{D_s}}^T \underline{\underline{\mathbf{K_s}}} \, \underline{\mathbf{D_s}} dx - w_{exter} = 0 \tag{45}$$

Considering that

$$\underline{\mathbf{D_s}} = \begin{bmatrix} B_a \\ B_s \\ B_b \end{bmatrix} \underline{\mathbf{\Phi}} = \underline{\underline{\mathbf{B}}}\ \underline{\mathbf{\Phi}} \tag{46}$$

the virtual work principle becomes:

$$\int_0^L \delta \underline{\mathbf{\Phi}}^T\ \underline{\underline{\mathbf{B}}}^T \underline{\underline{\mathbf{K_s}}}\ \underline{\underline{\mathbf{B}}}\ \underline{\mathbf{\Phi}} dx - w_{exter} = 0 \tag{47}$$

The section stiffness matrix presented hereafter is valid for homogeneous and non homogeneous sections even if the chosen axes are not the principal ones [GPP94]:

$$\underline{\underline{\mathbf{K_e}}} = \int_0^L \underline{\underline{\mathbf{B}}}^T \underline{\underline{\mathbf{K_s}}}\ \underline{\underline{\mathbf{B}}} dx \tag{48}$$

The numerical implementation of a multifiber beam is similar to a classical beam with the main difference that further loops are needed in the section level (scanning all the fibers) in order to construct the section stiffness matrix $\underline{\underline{\mathbf{K_s}}}$ [GPP94], [KM05], [MKRC06].

In the following chapter, a case study is presented on a reinforced concrete viaduct considering soil-structure interaction [GBKT11]. For this, a multifiber Timosheko beam is coupled with macro-elements [GKM09a], [GKM09b], [Gra13]. The reader can find other applications of the multifiber beam concept in the recent literature: non linear shear [CP94], non linear torsion [MKRC06], shaking table tests [KRM05], [INK+08], [GKM09c], retrofitting with fiber reinforced polymers [DMKP13]...

4 Case study: A reinforced concrete viaduct

5 Description of the structure

A 1:2.5 scaled viaduct was tested pseudo-dynamically in ELSA laboratory (JRC Ispra) (figure 6, [PVP+96]). Inertial forces were calculated numerically and imposed to the model piers through actuators by applying the adequate displacements. Details of the deck and piers are given (scaled) in figures 7(a) and 7(b). Piers are made of reinforced concrete and present hollow rectangular section shapes. The characteristics of the section of the deck are given in Table 1.

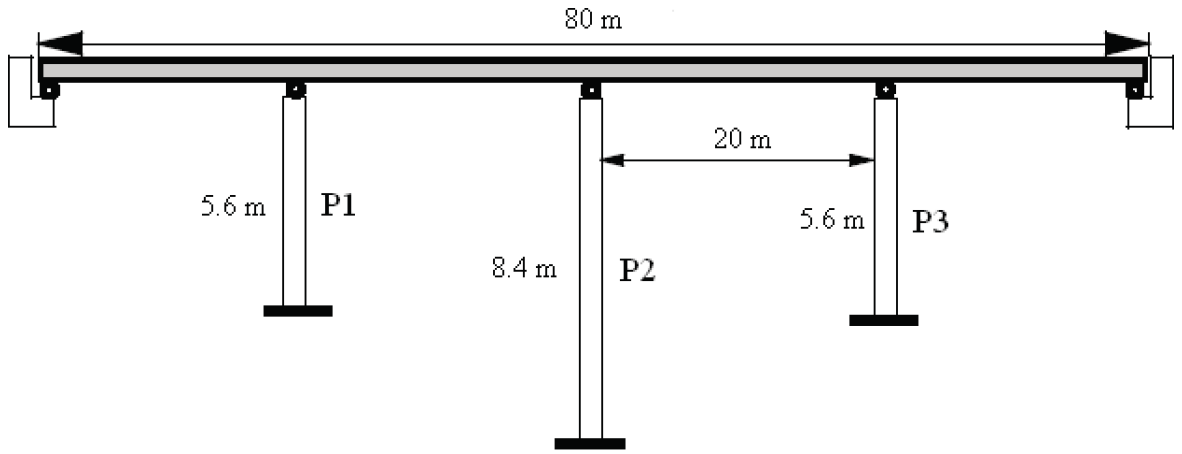

Figure 6: Viaduct: plan view (scale 1:2.5) [PVP+96].

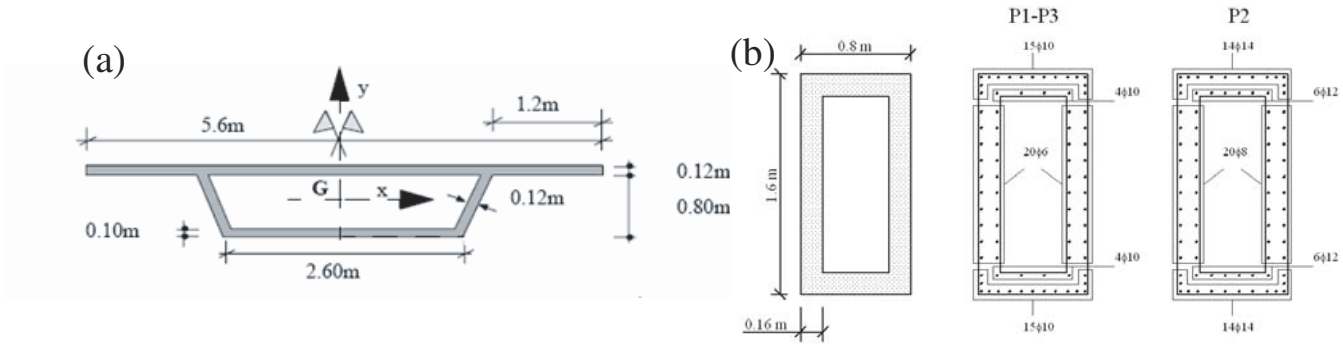

Figure 7: Viaduct: (a) deck, (b) piers (scale 1:2.5) [PVP+96].

Table 1: Viaduct: characteristics of deck cross section.

$A(m^2)$	$I_x(m^4)$	$I_y(m^4)$	$J(m^4)$
1.11	0.13	2.26	2.39

5.1 Finite element mesh

A finite element model using multifiber beams and concentrated masses is chosen to reproduce the structure (figure 8). The piers are at first considered fixed at the base. The mass and rotational inertia details are given in Table 2 [GBKT11].

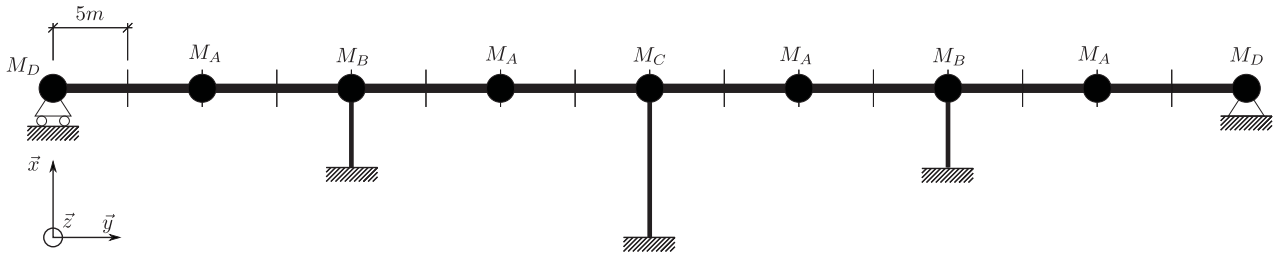

Figure 8: Viaduct: finite element mesh.

Table 2: Viaduct: masses and rotational inertia.

	Mass M (kg)	Rotational inertia I_x $(kg.m^2)$	Rotat. inertia I_z $(kg.m^2)$
M_A	27.5	285	234
M_B	32	287	271
M_C	34	288	322
M_D	13.75	143	117

Non linear Timoshenko multifiber beam elements are used to reproduce the behaviour of the piers [KM05], [MKRC06]. Six (6) elements are used for the piers P1 and P3 and nine (9) elements for the pier P2. Forty (40) concrete fibers and eighty (80) steel fibers are assumed in the sections, (figure 9). The deck is simulated using elastic linear beam elements. Calculations are made with FEDEASLab, a finite element MATLAB toolbox [FC04].

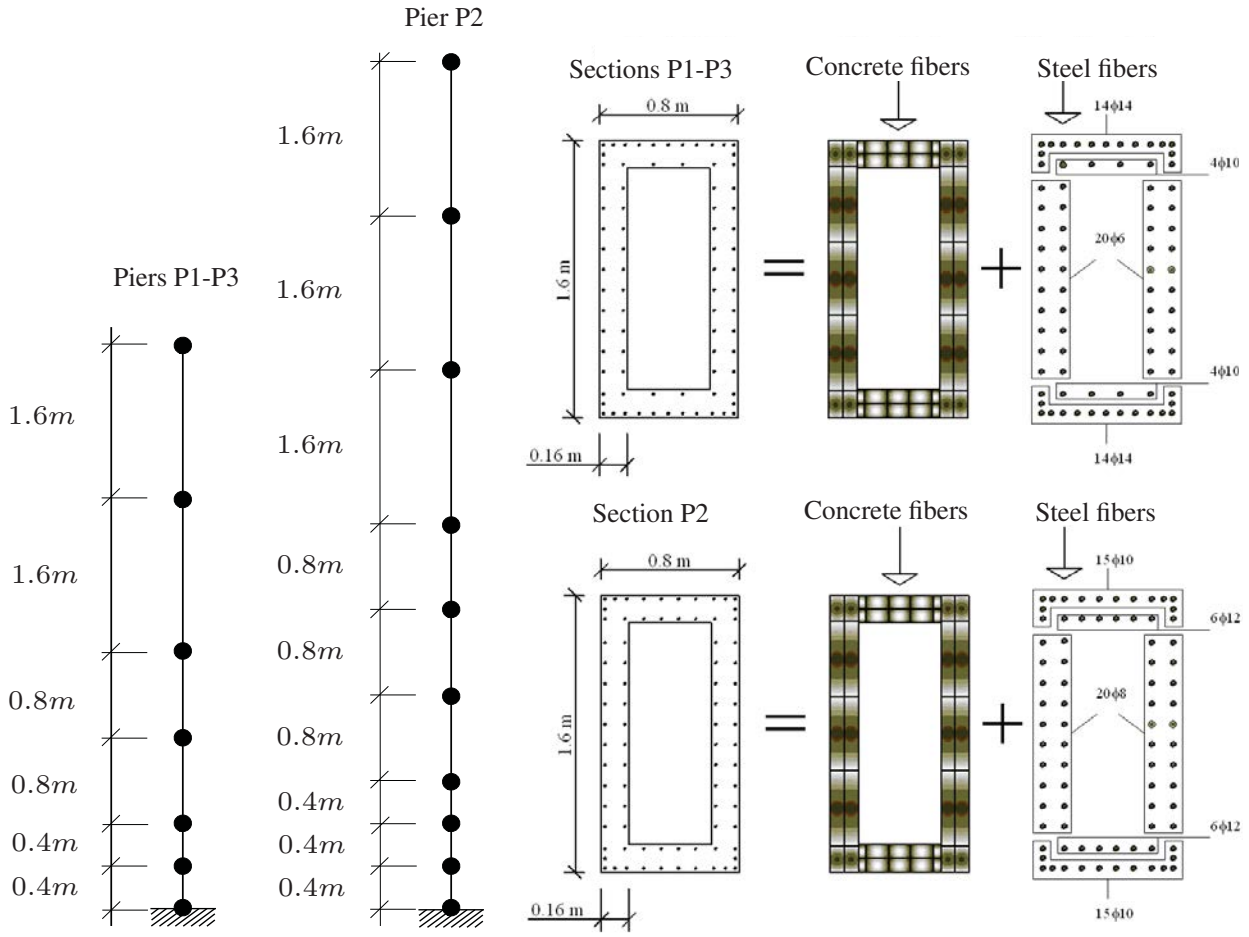

Figure 9: Viaduct: details of the multifiber beam element mesh (piers P1, P2 et P3).

5.2 Material parameters

A damage model with two scalar variables, one in compression and one in tension is adopted for concrete [LB91]. The model is able to reproduce the unilateral effect,

the permanent strains and the stiffness recovery. A modified version of the classical Menegotto-Pinto model [MP73] with an isotropic hardening is used for steel. It is worth noting that as the tests are pseudo-dynamic, the damping coefficient adopted in the numerical simulations has to be small [GBKT11].

5.3 Loading sequence

The accelerations imposed at the base of the structure derive from a synthetic accelerogram consistent with a 5% damping response specturm selected according to Eurocode 8 for a soil of class B. The peak of accelerations is situated at $0.35g$ ("weak" earthquake). A second similar accelerogram (dilated) is also imposed at the base of the structure. Its peak of acceleration is equal to $0.7g$ ("strong" earthquake) [GBKT11].

5.4 Experimental versus numerical results: dynamic analysis

Figures 10 and 11 show the comparison between the experimental and the numerical results of the dynamic analysis considering the piers fixed at the base. The two earthquakes (weak and strong) are imposed. The figures show the evolution with time of the shear forces at the base and the lateral displacements at the top of the piers P1, P2 and P3 [GBKT11].

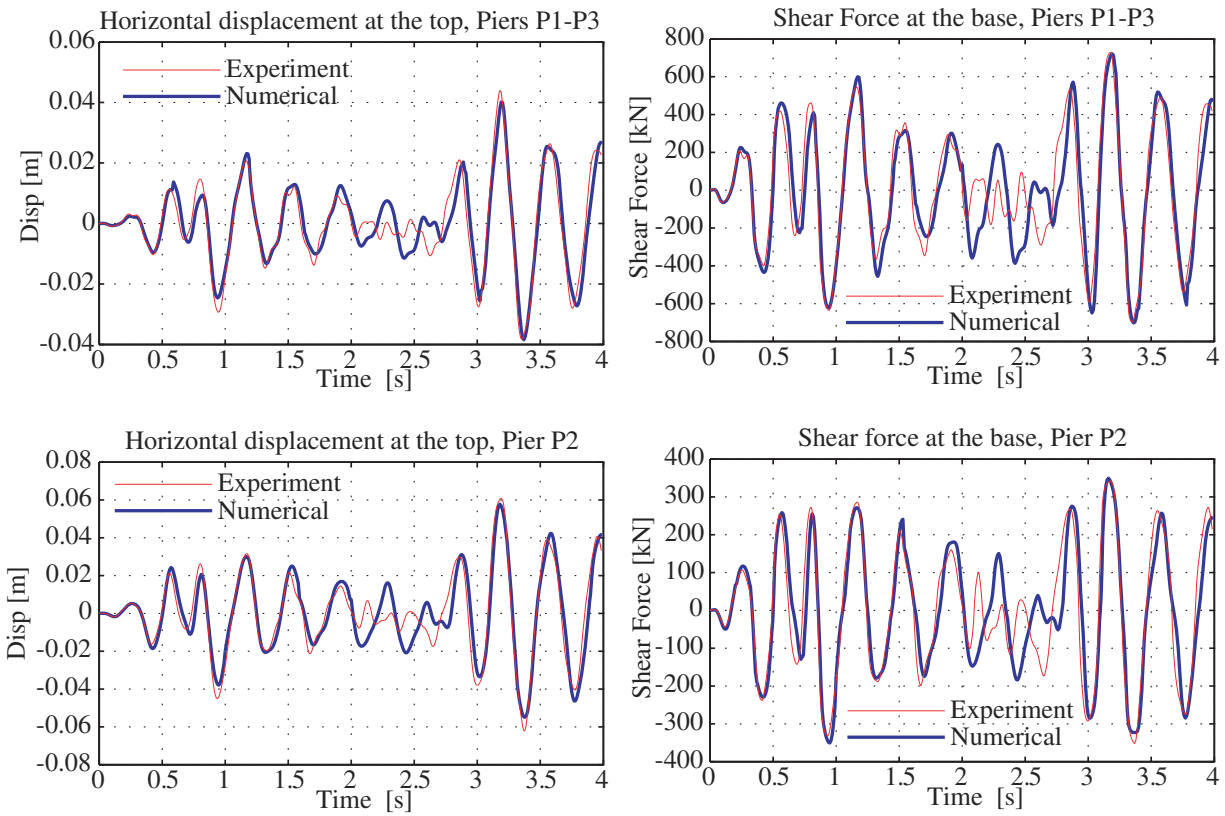

Figure 10: Viaduct - fixed base: comparison between experimental and numerical displacements and shear forces for the weak level earthquake [GBKT11].

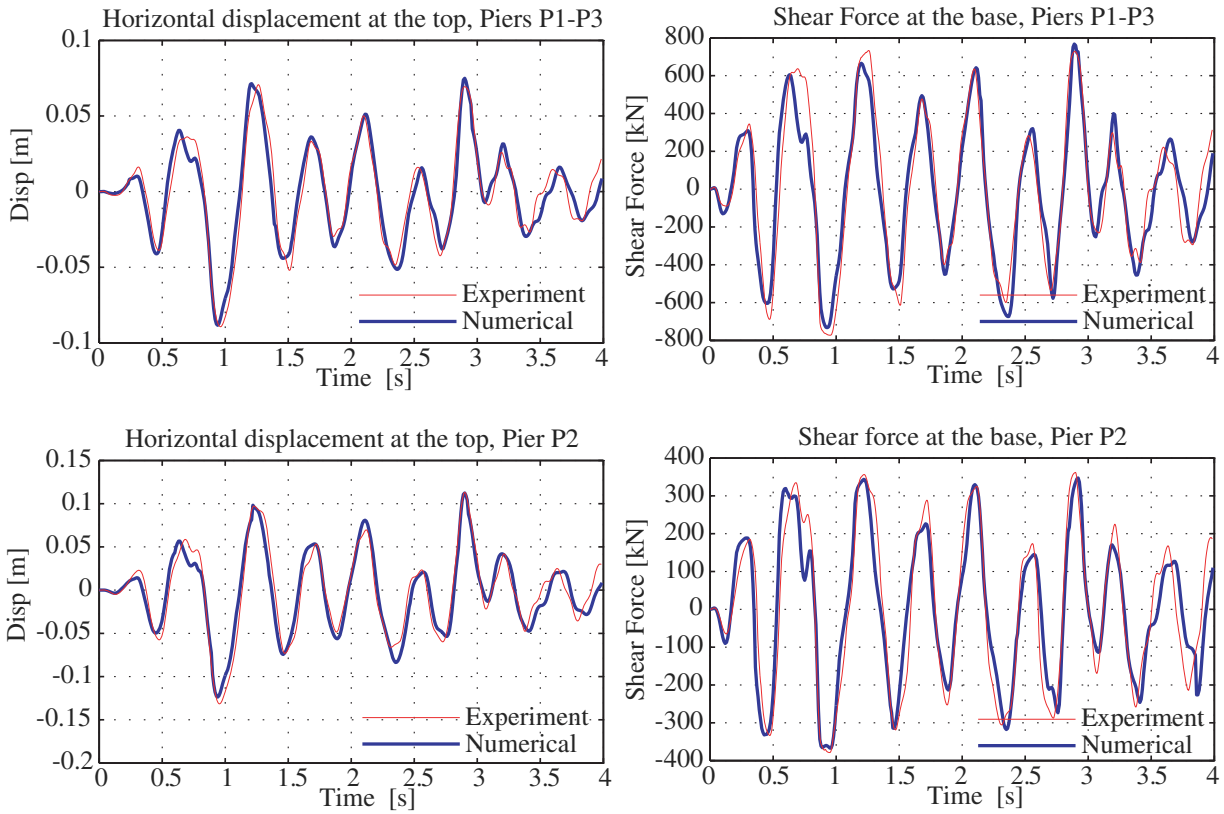

Figure 11: Viaduct - fixed base: comparison between experimental and numerical displacements and shear forces for the strong earthquake [GBKT11].

One can clearly see that despite the small number of degrees of freedom of the finite element model the non linear behaviour of the viaduct is reproduced quite satisfactorily. Not only the peaks in both directions are well reproduced but the frequency content of the response is correctly matched.

5.5 Dynamic analysis considering soil-structure interaction

Two modelling strategies are studied hereafter to take into account soil-structure interaction. The first uses the macro-element approach [GKM09a], [GKM09b], [Gra13] and the second linear elastic springs applied at the base of each pier. The elastic stiffness of the springs is calibrated such as that they accumulate the same energy as the non-linear macro-element [GBKT11]. The three types of boundary conditions are denominated hereafter as follows: linear springs (EL), macro-element (ME) and fixed (Fixed).

The results for the weak earthquake are presented in figure 12 for a class C soil. The predicted numerical behaviour of the viaduct differs depending on the assumed boundary conditions. The displacements are strongly amplified for the case of the structure resting on the macro-element and on the linear elastic springs. The results are more pronounced for the internal forces at the base of the piers (moments and shear forces). Loads on the structure are significantly reduced for the case of the macro-element.

Results obtained with the elastic linear springs are similar to the ones found for the fixed piers [GBKT11].

The limits of the classical engineering approach based on elastic linear springs are thus evident. For the case of the reinforced concrete viaduct internal forces and displacements are higher than the ones obtained using the macro-element, which allows a more appropriate description of the non linear behaviour of the foundation soil system.

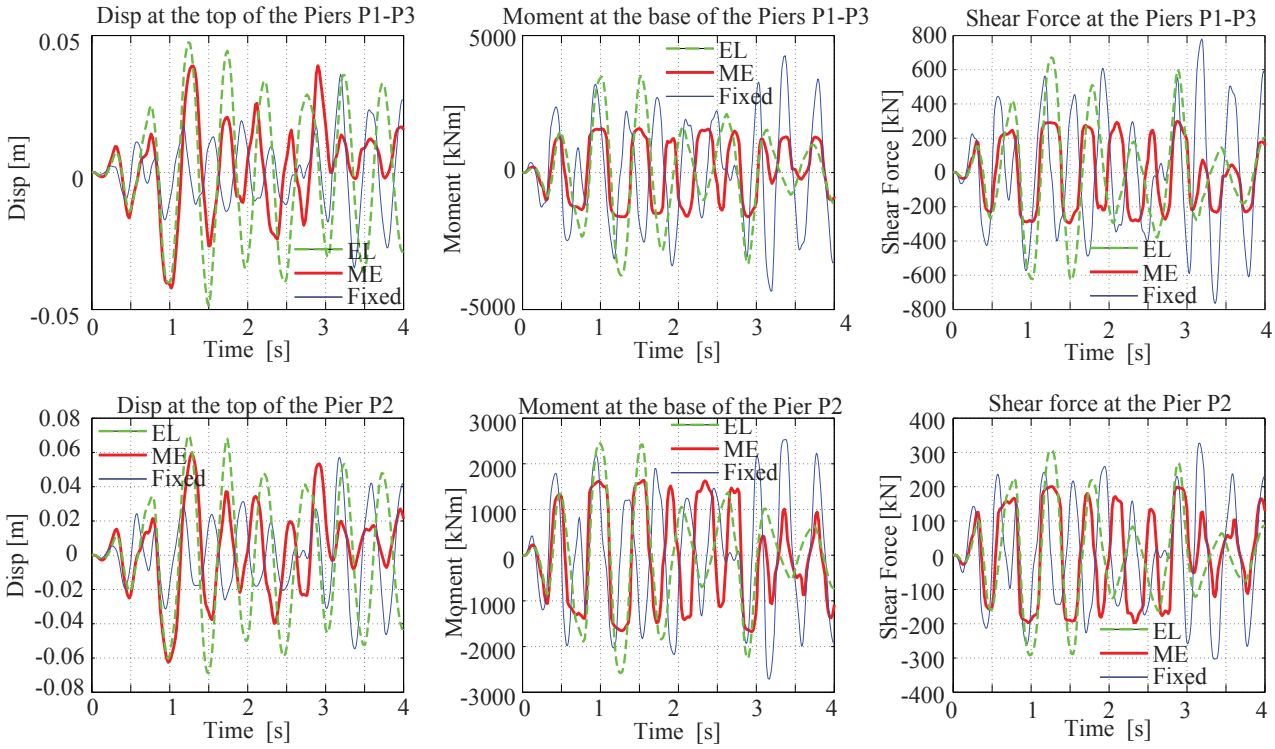

Figure 12: Viaduct - soil-structure interaction: comparison of the displacements, moments and shear forces for the weak motion and for a class C soil [GBKT11].

6 Conclusions

In this course, the formulation of a multifiber beam element was presented in detail. Adopting an Euler Bernoulli or a Timoshenko kinematic assumption, the element is able to reproduce the non linear behaviour of composite structures. A case study on a reinforced concrete viaduct subjected to earthquake loadings showed the performance of the approach. Combined with macro-elements [Gra13], it can take into account in a efficient, fast and robust way soil-structure interaction phenomena.

References

[Bit13] I. Bitar. Un nouvel élément fini poutre pour la modélisation des structures sous sollicitations complexes. Master thesis, Ecole Centrale de Nantes, 2013.

[CKCed] D. Caillerie, P. Kotronis, and R. Cybulski. An improved timoshenko finite element beam with internal degrees of freedom. *Finite Elements in Analysis and Design*, 2014 (submitted).

[Cow66] G.R. Cowper. The shear coefficient in timoshenko's beam theory. *Journal of Applied Mechanics*, 33(2):335–340, 1966.

[CP94] D. Combescure and P. Pegon. A fibre model accounting for transverse shear in castem 2000. Technical report, J.R.C., I-21020, Ispra, Italy, 1994. Special publication Nr. I.94.59.

[DL87] J. Donea and L.G. Lamain. A modified representation of transverse shear in c^0 quadrilateral plate elements. *Computer Methods in Applied Mechanics and Engineering*, 63(2):183 – 207, 1987.

[DMKP13] C. Desprez, J. Mazars, P. Kotronis, and P. Paultre. Damage model for frp-confined concrete columns under cyclic loading. *Engineering Structures*, 48(0):519 – 531, 2013.

[DVdG89] V. De Ville de Goyet. *L'analyse statique non linéaire par la méthode des éléments finis des structures spatiales formées de poutres à section non symétrique*. PhD thesis, Université de Liège, 1989.

[FC04] F.C. Filippou and M. Constantinides. Fedeaslab, getting started guide and simulations examples. Technical report, department of Civil and Environmental Engineering, UC Berkeley, 2004.

[FK93] Z. Friedman and J.B. Kosmatka. An improved two-node timoshenko beam finite element. *Computers & structures*, 47(3):473–481, 1993.

[Fre00] F. Frey. *Analyse des structures et milieux continus: mécanique des structures*, volume 2. PPUR, presses polytechniques et universitaires romandes, 2000.

[GBKT11] S. Grange, L. Botrugno, P. Kotronis, and C. Tamagnini. The effects of soil–structure interaction on a reinforced concrete viaduct. *Earthquake Engineering & Structural Dynamics*, 40(1):93–105, 2011.

[GKM09a] S. Grange, P. Kotronis, and J. Mazars. A macro-element to simulate 3d soil-structure interaction considering plasticity and uplift. *International Journal of Solids and Structures*, 46(20):3651 – 3663, 2009.

[GKM09b] S. Grange, P. Kotronis, and J. Mazars. A macro-element to simulate dynamic soil-structure interaction. *Engineering Structures*, 31(12):3034 – 3046, 2009.

[GKM09c] S. Grange, P. Kotronis, and J. Mazars. Numerical modelling of the seismic behaviour of a 7-story building: Nees benchmark. *Materials and structures*, 42(10):1433–1442, 2009.

[GPP94] J. Guedes, P. Pegon, and A. Pinto. A fibre timoshenko beam element in castem 2000. special publication nr. i.94.31. Technical report, J.R.C., I-21020, Ispra, Italy, 1994.

[Gra13] S. Grange. Simplified modeling strategies for soil-structure interaction problems: The macro-element concept. ALERT (The Alliance of Laboratories in Europe for Research and Technology) doctoral school on "Soil-Structure Interaction", ed. P. Kotronis, C. Tamagnini and S. Grange, 2013.

[HTK77] T.J.R. Hughes, R.L. Taylor, and W. Kanoknukulchai. A simple and efficient finite element for plate bending. *International Journal for Numerical Methods in Engineering*, 11(10):1529–1543, 1977.

[IF93] A. Ibrahimbegović and F. Frey. Geometrically non-linear method of incompatible modes in application to finite elasticity with independent rotations. *International journal for numerical methods in engineering*, 36(24):4185–4200, 1993.

[INK+08] N. Ile, X.H. Nguyen, P. Kotronis, J. Mazars, and J.M. Reynouard. Shaking table tests of lightly rc walls: Numerical simulations. *Journal of Earthquake Engineering*, 12(6):849–878, 2008.

[IW91] A. Ibrahimbegovic and E.L. Wilson. A modified method of incompatible modes. *Communications in Applied Numerical Methods*, 7(3):187–194, 1991.

[KM05] P. Kotronis and J. Mazars. Simplified modelling strategies to simulate the dynamic behaviour of r/c walls. *Journal of Earthquake Engineering*, 9(02):285–306, 2005.

[KRM05] P. Kotronis, F. Ragueneau, and J. Mazars. A simplified modelling strategy for r/c walls satisfying ps92 and ec8 design. *Engineering Structures*, 27(8):1197–1208, 2005.

[LB91] C. La Borderie. *Phénomènes unilatéraux dans un matériau endommageable: modélisation et application l'analyse des structures en béton.* PhD thesis, Université Paris 6, 1991.

[MKRC06] J. Mazars, P. Kotronis, F. Ragueneau, and G. Casaux. Using multifiber beams to account for shear and torsion: Applications to concrete struc-

tural elements. *Computer Methods in Applied Mechanics and Engineering*, 195(52):7264–7281, 2006.

[MP73] M. Menegotto and P. Pinto. Method of analysis of cyclically loaded reinforced concrete plane frames including changes in geometry and non-elastic behaviour of elements under combined normal force and bending. In *IABSE Symposium on resistance and ultimate deformability of structures acted on by well-defined repeated loads, final report, Lisbon*, page 328p, 1973.

[OH80] D.R.J. Owen and E. Hinton. *Finite elements in plasticity: Theory and practice*. Pineridge Press Ltd, Swansea, England, 1980.

[Peg94] P. Pegon. A timoshenko simple beam element in castem 2000. Technical report, J.R.C., I-21020, Ispra, Italy, 1994. special publication Nr. I.94.04.

[PVP+96] A.V. Pinto, G. Verzeletti, P. Pegon, G. Magonette, P. Negro, and J. Guedes. Pseudo dynamic testing of large-scale r/c bridges. Technical report, HMC grant holder report EUR 16378 EN, 1996.

[SFT96a] E. Spacone, F.C. Filippou, and F.F. Taucer. Fiber beam-column model for nonlinear analysis of r/c frames. i: Formulation. *Earthquake Engineering and Structural Dynamics*, 25(7):711–725, 1996.

[SFT96b] E. Spacone, F.C. Filippou, and F.F. Taucer. Fiber beam-column model for nonlinear analysis of r/c frames. ii: Applications. *Earthquake Engineering and Structural Dynamics*, 25(7):727–742, 1996.

[ZT05] O.C. Zienkiewicz and R. L. Taylor. *The finite element method for solid and structural mechanics*. Butterworth-Heinemann, 2005.